

Simultaneous Boron Ion-Channel/Growth Factor Receptor Activation for Enhanced Vascularization

Patricia Rico,* Aleixandre Rodrigo-Navarro, Marcos de la Peña, Vladimira Moulisová, Mercedes Costell, and Manuel Salmerón-Sánchez*

Boron ion is essential in metabolism and its concentration is regulated by ion-channel NaBC1. NaBC1 mutations cause corneal dystrophies such as Harboyan syndrome. Here a 3D molecular model for NaBC1 is proposed and it is shown that simultaneous stimulation of NaBC1 and vascular endothelial growth factor receptors (VEGFR) promotes angiogenesis *in vitro* and *in vivo* with ultralow concentrations of VEGF. Human umbilical vein endothelial cells' (HUVEC) organization into tubular structures is shown to be indicative of vascularization potential. Enhanced cell sprouting is found only in the presence of VEGF and boron, the effect abrogated after blocking NaBC1. It is demonstrated that stimulated NaBC1 promotes angiogenesis via PI3k-independent pathways and that $\alpha_5\beta_1/\alpha_v\beta_3$ integrin binding is not essential to enhanced HUVEC organization. A novel vascularization mechanism that involves crosstalk and colocalization between NaBC1 and VEGFR receptors is described. This has important translational consequences; just by administering boron, taking advantage of endogenous VEGF, *in vivo* vascularization is shown in a chorioallantoic membrane assay.

of cells and tissues as they are permeated with hierarchical blood vessels that provide oxygenation and nutrients and remove toxic metabolites. Besides promoting multiple vital cell functions, vascularization is a fundamental process involved in inflammation, tumor growth and metastasis, which is regulated by vascular endothelial growth factor (VEGF) via interaction with its receptor (VEGFR).^[2]

Current strategies to promote vascularization are based on using growth factors (GFs), from simple delivery systems to highly engineered synergistic bioactive materials.^[3,4] However, despite efforts, strategies based on GF delivery normally require the use of high concentrations to prevent their low stability and limited mode of action. For example, in a preliminary evaluation of phase I trial on the safety of topical administration of VEGF for the treatment of diabetic ulcers,

72 $\mu\text{g cm}^{-2}$ every 48 h for up to 6 weeks was considered "well tolerated" and no toxic despite the high doses used.^[5] GFs possess high capability to induce intracellular signaling but they also play an essential role in tumor growth, invasion, and metastasis. Therefore, the use of supraphysiological doses of GFs may produce serious adverse side effects such as reported by the Food and Drug Administration (FDA) for recombinant

1. Introduction

Vasculogenesis, *de novo* development of new blood vessels from precursor cells, and angiogenesis, organization, and remodeling from pre-existing ones are both essential processes contributing to development of vascular systems.^[1] Entirely developed vascular networks are essential for the functionality

Dr. P. Rico, Prof. M. Salmerón-Sánchez
Biomedical Research Networking Center in Bioengineering
Biomaterials and Nanomedicine (CIBER-BBN)
Universitat Politècnica de València
Camino de Vera s/n, 46022 Valencia, Spain
E-mail: parico@upvnet.upv.es; Manuel.Salmeron-Sanchez@glasgow.ac.uk

Dr. P. Rico, Prof. M. Salmerón-Sánchez
Center for Biomaterials and Tissue Engineering (CBIT)
Universitat Politècnica de València
Camino de Vera s/n, 46022 Valencia, Spain

Dr. A. Rodrigo-Navarro, Dr. V. Moulisová, Prof. M. Salmerón-Sánchez
Centre for the Cellular Microenvironment
School of Engineering
University of Glasgow
G12 8LT Glasgow, UK

Dr. M. de la Peña
Instituto de Biología Molecular y Celular de Plantas
Centro Superior de Investigaciones Científicas (CSIC)
Universitat Politècnica de València
Camino de Vera s/n, 46022 Valencia, Spain

Dr. V. Moulisová
Biomedical Center
Faculty of Medicine in Pilsen
Charles University
Alej Svobody 76, 32300 Pilsen, Czech Republic

Dr. M. Costell
Departament de Bioquímica i Biologia Molecular
Universitat de València
Doctor Moliner s/n, 46100 Burjassot, Spain

 The ORCID identification number(s) for the author(s) of this article can be found under <https://doi.org/10.1002/adbi.201800220>.

DOI: 10.1002/adbi.201800220

human bone morphogenetic protein 2 (rhBMP2)-infuse,^[6] or platelet-derived growth factor (PDGF) (Regranex).^[7] Thus, alternative strategies that avoid the use of GFs or the use of very low dosages are needed to improve current therapies.

Angiogenesis is a tightly regulated process controlled by the dynamic interplay between GFs, extracellular matrix (ECM), and integrins.^[8] Integrins are a family of transmembrane glycoproteins that activate after binding to a high repertoire of ECM components such as fibronectin (FN), collagen, laminin, fibrinogen (FG), or other surface receptors, and mediate mechanical forces and biochemical signals—they are mechanosensors that regulate multiple cellular events.^[9] The importance of the interplay between integrins and GF receptors has been extensively demonstrated^[10,11] as well as the interplay between GF receptors, integrins, and other transmembrane proteins such as urokinase plasminogen activator (uPA) receptor (uPAR).^[12,13]

Ion channels are integral membrane proteins that control the ion flow through the cells, and besides regulating cell homeostasis, they can act as mechanosensors communicating extracellular signals to both the cytoplasmic environment^[14] and integrins.^[15] Only recently it has been reported the role of some calcium and potassium channels as potential therapeutic targets for cancer due to their importance in tumor vascularization.^[16] Calcium channels play a major role in angiogenesis being part of signaling pathways linked to VEGF and its receptors VEGFR1/VEGFR2.^[17] Sodium boron cotransporter 1 (NaBC1 encoded by BTR1 or SLC4A11 gene) controls boron (B) homeostasis. Little is known about homeostasis and the function of this metalloid that plays a key role in the metabolism of plant and mammalian cells. We have previously reported that boron enhances myogenic differentiation.^[18]

NaBC1 is unique among members of the SLC4 family of sodium-coupled bicarbonate transporter proteins. In the absence of borate, NaBC1 conducts Na⁺ and OH⁻ (H⁺), while in the presence of borate, NaBC1 functions as an electrogenic Na⁺-coupled borate cotransporter.^[19] Mutations in NaBC1 gene cause genetic diseases either affecting the cornea and eventually producing blindness (congenital hereditary endothelial corneal dystrophy (CHED), Fuchs endothelial corneal dystrophy (FECD)) or a combined corneal dystrophy plus sensorineural deafness (Harboyan syndrome (HS)).^[20,21]

Here, we report a novel mechanism by which boron induces angiogenesis in vitro and in vivo via simultaneous NaBC1 and VEGFR activation using ultralow doses of soluble VEGF (<5 ng cm⁻², compared to, e.g., 72 μg cm⁻² administered in clinical trials) (Figure 1a).

2. Results

2.1. Boron Transporter (NaBC1): 3D Molecular Modeling and Expression

The protein encoded by the SLC4A11 gene (also named BTR1 or NaBC1) was originally identified as a possible bicarbonate transporter.^[22] Notably, it was recently characterized as a sodium–boron cotransporter which is essential for mediating effect of boron in mammalian cells.^[19] Multiple alignments of polypeptide sequences with representative members of

bicarbonate transporters family (AE4, NBC1, and NDCBE1) are shown in Figure S1 (Supporting Information). Based on the best topology match, of ≈30%, in the PDB database corresponding to human erythrocyte band 3 protein SLC4A1, we predicted a 3D-protein structural model of *Homo sapiens* bicarbonate transporter-related protein NaBC1 (Figure 1b).

Most of the predicted transmembrane spans and intracellular phosphorylation sites previously reported as targets for different protein kinases^[22] are present in the protein sequence used for the predicted 3D model of NaBC1. Their relative positions are shown in Figure S1 (Supporting Information).

In order to confirm the expression of NaBC1 in our cellular system, we amplified human umbilical vein endothelial cells (HUVEC) NaBC1 messenger ribonucleic acid (mRNA) by polymerase chain reaction (PCR). We have used specific primers designed to avoid genomic amplification and located at the end and the beginning of two contiguous exons. Figure 1c shows the detected band of 238 nucleotides corresponding to mRNA of NaBC1 in all substrates. The presence of the bands observed in all conditions confirms that NaBC1 is ubiquitously expressed in HUVEC, as in other cellular systems.^[19]

NaBC1 transporter is boron specific and functions as an electrogenic obligated Na⁺-coupled borate cotransporter in the presence of borate. In the absence of borate, NaBC1 conducts Na⁺ and OH⁻ (H⁺). As we have used sodium tetraborate decahydrate (borax) in this work, boron uptake by cells must occur via NaBC1 transporter, thus, via ion-channel activation instead of any other alternative transport mechanisms such as passive diffusion through the cell membrane, as for, e.g., boric acid.^[23]

2.2. NaBC1 Stimulation Promotes HUVEC Organization

Having cells attached on a fibronectin-coated poly(L-lactic acid) (PLLA) surface, we examined the ability of boron to induce organization of endothelial cells into tubular-like structures in the presence or absence of very low soluble doses of VEGF (25 ng mL⁻¹). Note that we have used PLLA surfaces in vitro to be consistent with the carrier used afterwards in vivo. Also, as it is known that 3D-like environments are important to support vascularization,^[3] after cell seeding on PLLA, samples were covered with a thin layer of fibrin matrix that provided cells with a simple 3D environment to support HUVEC sprouting and organization into cellular networks (Figure S2 in the Supporting Information shows HUVEC behavior in 2D conditions). After 6 days, cells cultured with boron (B2% and B5%) and VEGF supplemented media revealed enhanced network formation compared to cells cultured only with VEGF supplemented media (Figure 2a, first and second rows). Image analysis revealed statistical significant differences that support the hypothesis that boron promotes vascularization effectively only in combination with VEGF (Figure 2b). Cell organization into tubular structures was quantified using parameters such as cell number, percentage of area covered by cells, number of aligned structures, total length of aligned structures, and the number of junctions (detailed process of image analysis quantification is shown in Figure S3 in the Supporting Information).

Total cell number was similar in all conditions (B0%, B2%, and B5%), but with significant higher values when VEGF was added into the culture medium (Figure S4a—cell number,

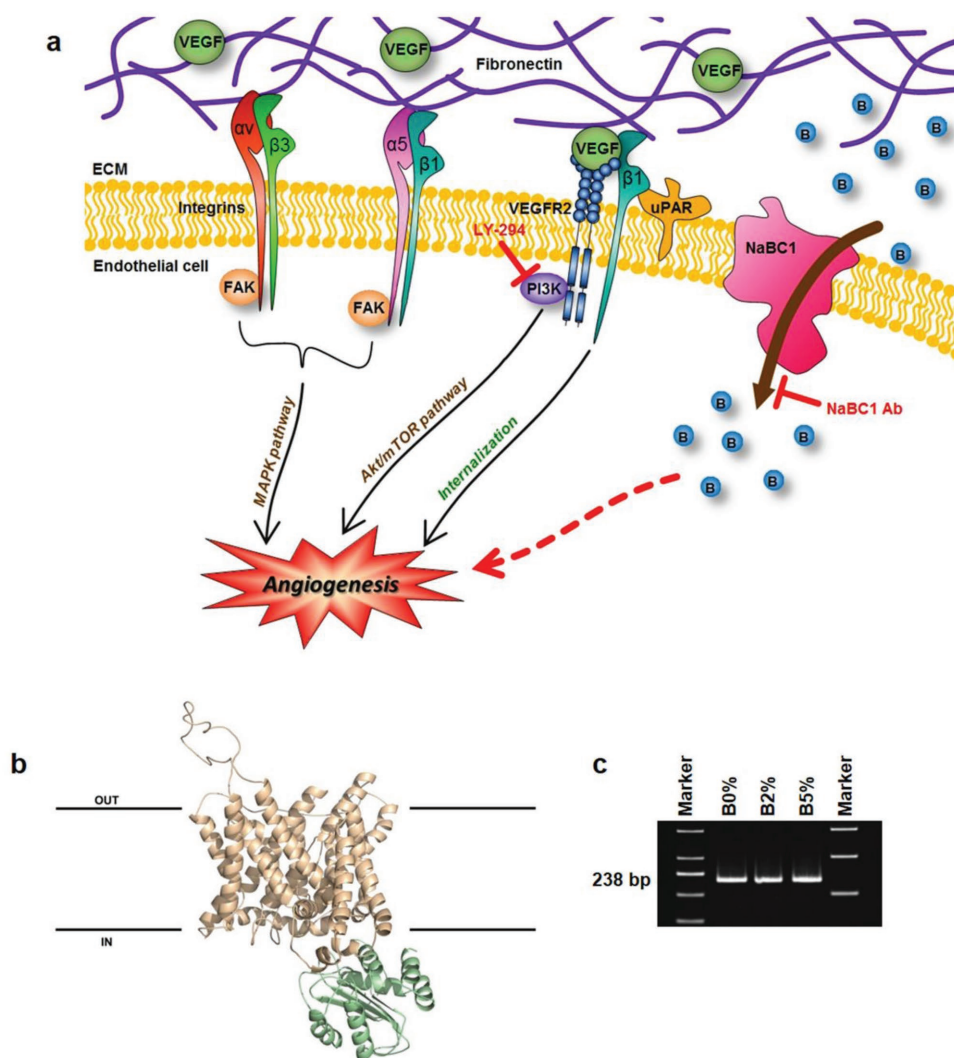


Figure 1. The NaBC1 transporter. a) Schematic picture of events representing the role of boron and NaBC1 transporter, as well as other membrane receptors, in the regulatory crosstalk promoting vasculogenesis. b) Predicted structural 3D model of NaBC1 transporter based on the best topology match corresponding to human erythrocyte band 3 protein SLC4A1. The cytosolic and the anion exchanger domains are shown in green and yellow, respectively. The relative positions of both domains were placed arbitrarily. c) PCR amplification of NaBC1 mRNA of 238 nt extracted from HUVEC seeded onto different substrates with different amounts of boron. Left marker 50 bp, right marker 100 bp.

Supporting Information). Equally, the percentage of area covered by cells followed a similar trend, with comparable values among the three conditions that increase in cultures supplemented with VEGF (Figure S4a—percentage of area covered by cells, Supporting Information).

The number of aligned structures was similar for B0% and + VEGF; however, it strongly diminished for B2% and B5% when VEGF was added (Figure 2b, first row, number of aligned structures). Lower number of aligned structures involves more cocontinuity of tubular structures, with a higher number of junctions (Figure 2b, first row, number of junctions) and total length of structures (Figure S4a—total length, Supporting Information). Overall, these parameters suggest higher levels of HUVEC organization when cells are cultured in the presence of boron and VEGF and suggest cooperation between boron transporter NaBC1 and VEGF receptor (Figure 1a).

2.3. NaBC1 Blocking Inhibits HUVEC Organization and Sprouting

As boron was only effective in combination with VEGF (Figure 2a, first and second rows), we have used media containing ultralow doses of VEGF (25 ng mL^{-1}) in all experiments from now on. We first investigated the role of boron by inhibiting the NaBC1 transporter using a specific antibody. Blocking NaBC1 resulted in reduced cellular organization (Figure 2a, third row) as quantified by image analysis (Figure 2b, second row); the number of aligned structures increased whereas their total length and the number of junctions diminished only for cells cultured with boron in the media (B2% and B5%; Figure 2b; Figure S4b, Supporting Information). Note that the total cell number and fraction of area covered by cells decreased in all conditions after blocking NaBC1 (Figure S4b, Supporting Information).

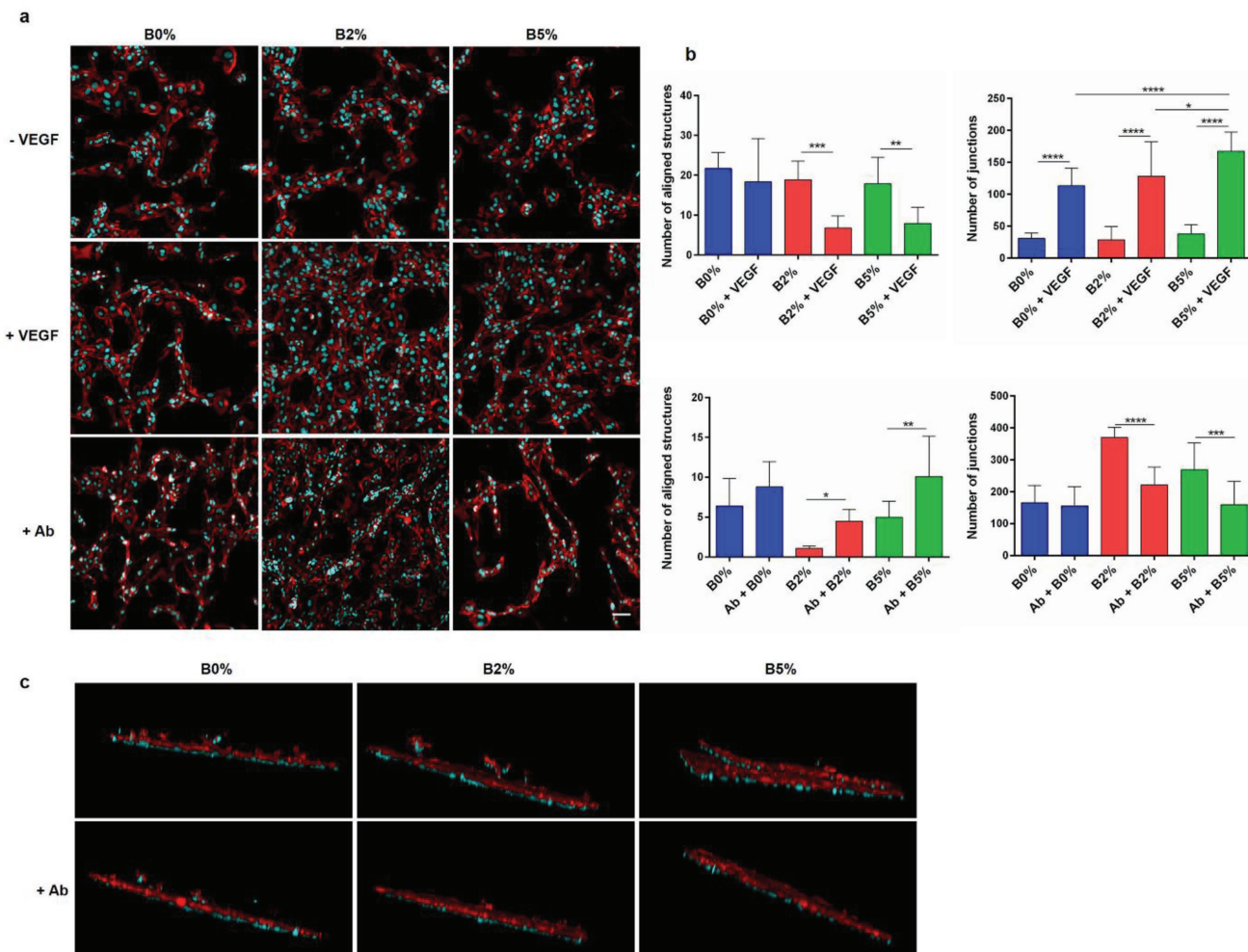


Figure 2. HUVEC organization in 3D fibrin matrix environments. a) Fluorescence images of actin cytoskeleton (red) and nuclei (cyan) of HUVEC cultured during 6 days onto functionalized substrates (FN-coated) and with or without VEGF (25 ng mL^{-1}) and boron (B0%, B2%, and B5%) present in the culture medium. B2% and B5% substrates showed higher degree of cell organization compared to B0% (first and second rows). Effects of NaBC1 blocking on HUVEC organization. HUVEC cultured during 6 days onto functionalized substrates (FN-coated), with VEGF (25 ng mL^{-1}) and boron (B0%, B2%, and B5%) present in the culture medium, after blocking with a specific NaBC1 antibody. NaBC1 blocking prevented cell organization on B2% and B5% conditions (third row). Scale bar represents $100 \mu\text{m}$. b) Image analysis quantification of different parameters related to HUVEC organization. Boron induces the formation of HUVEC network structures in combination with VEGF, leading to the minimal number of aligned structures (i.e., most of the structure are connected) and the higher number of junctions (first row). Image analysis quantification of parameters related to HUVEC organization after blocking the NaBC1 transporter (second row). The number of aligned structures augmented, the total length, and the number of junctions diminished suggesting impaired network organization only in the presence of boron. Statistics are shown as mean \pm standard deviation. $N = 10$ images per condition from three different biological replicas. Data were analyzed by an ordinary one-way ANOVA test and corrected for multiple comparisons using Sidak's analysis ($p = 0.05$). $*p < 0.05$, $**p < 0.01$, $***p < 0.001$, $****p < 0.0001$. c) Confocal 3D images of HUVEC sprouting into 3D fibrin matrix deposited onto functionalized substrates (FN-coated), with VEGF (25 ng mL^{-1}) and boron (B0%, B2%, and B5%) present in the culture medium, after pre-incubation with specific NaBC1 antibody—actin cytoskeleton (red) and nuclei (cyan). Sprouting is not observed when NaBC1 is blocked. For 3D movies, see Videos S1–S6 (Supporting Information) of sproutings.

We then looked at cell sprouting into the fibrin matrix that was used to cover cells and provide a supporting 3D environment.^[3] Cell sprouting eventually occurred in all substrates (B0%, B2%, and B5%); however, it was enhanced only in the presence of VEGF and boron (B2% and B5%) (Figure 2c; Videos S1–S6, Supporting Information). Accordingly, blocking of NaBC1 inhibited this enhanced cell sprouting only in the presence of boron (B2% and B5%). This result demonstrates that boron activation of NaBC1 is key in promoting cell migration and matrix remodeling (Figure 2c).

2.4. NaBC1 Stimulation Compensates PI3k/Akt Signaling

We next investigated whether angiogenesis triggered by boron activation of NaBC1 involved downstream phosphorylation of PI3k/Akt, a pathway typically associated with VEGF signaling^[24] (Figure 3a). In cell western assay showed that NaBC1 activation in combination with VEGF induced significantly Akt phosphorylation (Figure 3b). PI3k inhibition using 2-(4-morpholinyl)-8-phenyl-1(4*H*)-benzopyran-4-one hydrochloride (LY-294002) strongly diminished HUVEC

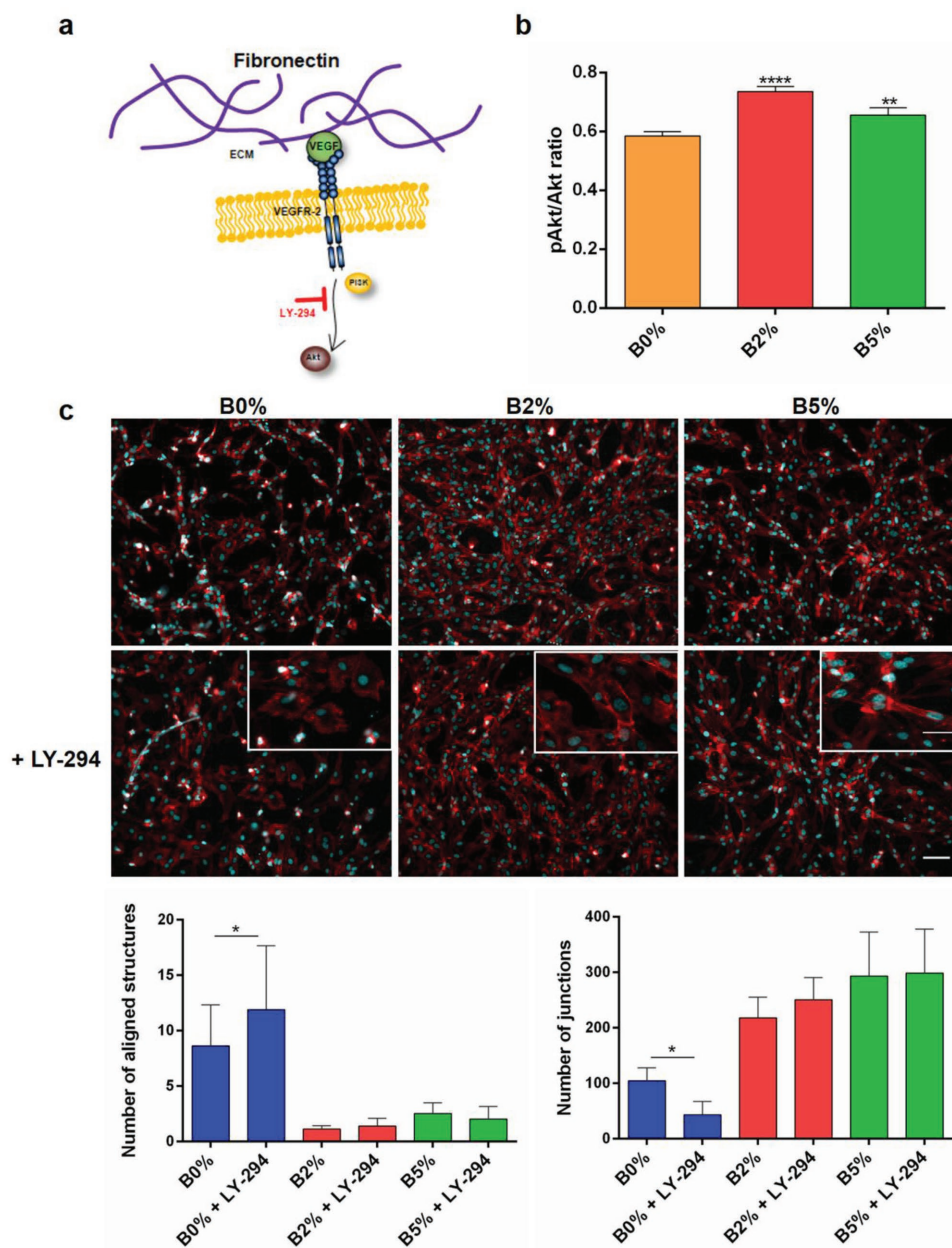


Figure 3. Effects of PI3k inhibition on HUVEC organization. a) Schematic representation of mode of action of LY-294002 inhibitor. b) In cell western assay showing pAkt/Akt ratio on HUVEC after 45 min of culture. NaBC1 stimulation in the presence of VEGF resulted in significant enhancement of Akt phosphorylation. Statistics are shown as mean \pm standard deviation. $N = 4$ biological replicas. Data were analyzed by an ordinary one-way ANOVA test and corrected for multiple comparisons using Dunnett analysis ($p = 0.05$). $**p < 0.01$, $****p < 0.0001$. c) Images of actin cytoskeleton (red) and nuclei (cyan) of HUVEC cultured during 6 days onto functionalized substrates (FN-coated) with VEGF (25 ng mL^{-1}) and boron (B0%, B2%, and B5%) present in the culture medium after 1 day of incubation with PI3k inhibitor. The upper row was considered as a culture control. Scale bar represents 100 and 50 μm for magnification images. Image analysis quantification of parameters related to HUVEC organization. PI3k blocking did not influence HUVEC network formation in the presence of boron. Statistics are shown as mean \pm standard deviation. $N = 10$ images per condition from three different biological replicas. Data were analyzed by an ordinary one-way ANOVA test and corrected for multiple comparisons using Sidak's analysis ($p = 0.05$). $*p < 0.05$, $****p < 0.0001$.

organization (Figure 3c, B0%) but did not influence HUVEC alignment and fusion in the presence of boron (B2% and B5%, Figure 3c, magnification images). Image analysis showed that LY-294002 reduced significantly cell number in all cases notwithstanding percentage of area covered by cells, number and total length of structures, as well as number

of junctions remained invariable in the presence of boron (Figure 3c graphics and Figure S3c, Supporting Information). HUVEC organization triggered by boron stimulation of NaBC1 in the presence of LY-294002 suggests that active NaBC1 compensates PI3k inhibition, by stimulation of Akt signaling downstream of PI3k.

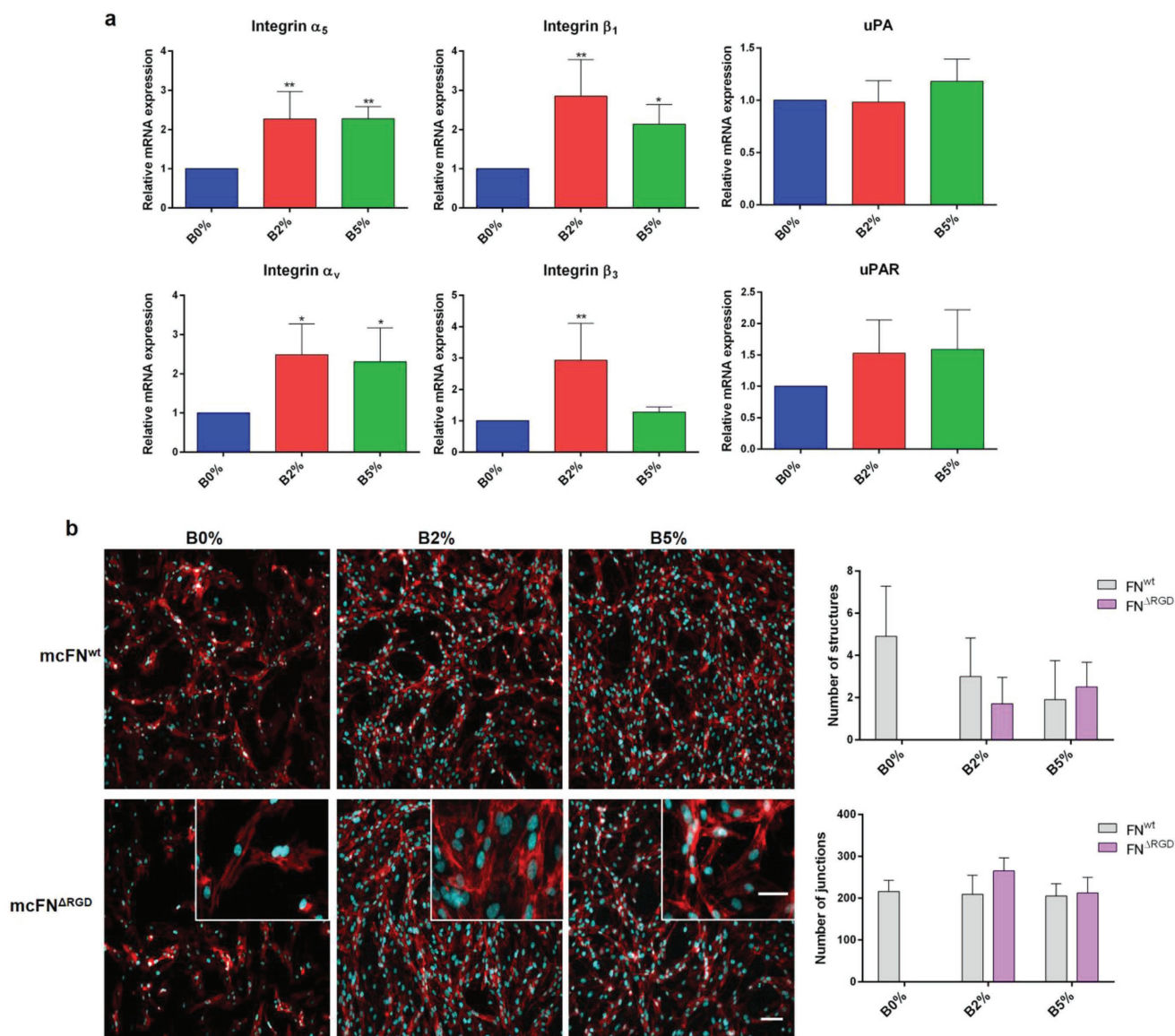


Figure 4. Gene expression of membrane receptors and effects of FN-binding domains in HUVEC organization. a) Analysis of relative mRNA expression of receptors involved in vascularization. The presence of boron enhanced the expression of $\alpha_5\beta_1$ and $\alpha_V\beta_3$ integrins and uPAR. Statistics are shown as mean \pm standard deviation. $N = 5$ different biological replicas. Data were analyzed by an ordinary one-way ANOVA test and corrected for multiple comparisons using Dunnett analysis ($p = 0.05$). * $p < 0.05$, ** $p < 0.01$. b) Effects of FN^{ARGD} mutation in HUVEC organization. Fluorescence images of actin cytoskeleton (red) and nuclei (cyan) of HUVEC cultured during 6 days onto functionalized substrates mutant FN-coated, with VEGF (25 ng mL⁻¹) and boron (B0%, B2%, and B5%) present in the culture medium. Impaired binding of $\alpha_5\beta_1$ and $\alpha_V\beta_3$ integrins (cells grown onto FN^{ARGD}) resulted in lack of HUVEC organization on B0% substrates (magnification images showing formation or not of tubular-like network). Interestingly, the presence of boron compensates the integrin binding maintaining led to unaltered levels of HUVEC organization levels. For image analysis quantification of different parameters related to HUVEC organization, see Figure S5d in the Supporting Information. Scale bar represents 100 and 50 μ m for magnification images. Data are represented as mean \pm standard deviation. $N = 10$ images per condition from three different biological replicas.

2.5. Effect of NaBC1 Activation in the Expression of Other Membrane Receptors Involved in Vascularization

We have shown that boron stimulates NaBC1 and, in the presence of ultralow doses of VEGF, promotes enhanced HUVEC organization and sprouting. Next, we investigated whether boron activation of NaBC1 influences the expression of other relevant receptors. Previous studies reported the critical role of integrin $\alpha_5\beta_1$ and $\alpha_V\beta_3$ in angiogenesis and vascular

development^[25–27] and uPA—an ECM protease—and uPAR in endothelial cell migration in response to VEGF.^[12]

Quantification of gene expression by quantitative PCR (qPCR) revealed enhanced integrin $\alpha_5\beta_1$ and $\alpha_V\beta_3$ as well as uPAR with no effect on uPA levels (Figure 4a for B2% and B5%). Because uPAR,^[13] β_1 ,^[28] and β_3 ^[29] integrins are known to cooperate with VEGFR to induce angiogenesis, our data suggest a novel signaling mechanism that involves cooperation between NaBC1 (boron activated) and VEGFR (VEGF activated)

leading to enhanced expression of $\alpha_5\beta_1/\alpha_v\beta_3$ integrins and uPA receptors (Figure 1a).

2.6. Simultaneous NaBC1 and VEGFR Signaling is Not $\alpha_5\beta_1/\alpha_v\beta_3$ Dependent

To further investigate the interplay between NaBC1 and integrin receptors in HUVEC organization we used mutant fibronectins that compromise $\alpha_5\beta_1$ and $\alpha_v\beta_3$ integrin binding. Mutations in FN^{RGE} and FN^{ARGD} are located in the FN tenth type III module (FNIII₁₀, RGD motif) and impair binding of $\alpha_5\beta_1$ or $\alpha_5\beta_1/\alpha_v\beta_3$ respectively. Mutations in FN^{syn} are located in the synergy site (DRVPHSRN motif) located in the FN ninth type III module (FNIII₉) in close proximity to the RGD motif. The synergy site binds $\alpha_5\beta_1$ but not α_v -class integrins; thus, mutations in this site results in low binding affinity for $\alpha_5\beta_1$.^[30]

Since we have used mouse cellular fibronectins (mcFNs), we first confirmed the same HUVEC organization using wild-type mcFN (mcFN^{wt}) compared to human plasma FN (hpFN) (Figure S5a,b, Supporting Information). Experiments with mutant mcFN confirmed that albeit enhanced expression of $\alpha_5\beta_1$ and $\alpha_v\beta_3$ integrins, this is independent of vasculogenesis triggered by simultaneous NaBC1/VEGFR signaling. mcFN^{syn} led to unaltered HUVEC organization compared to mcFN^{wt}, with still B2% and B5% presenting the best levels of tubular-like network formation even if $\alpha_5\beta_1$ binding is prevented (Figure S5c, second row, Supporting Information). Using mcFN^{RGE} and mcFN^{ARGD} (that prevent both $\alpha_5\beta_1$ and α_v binding) still allowed cells organization into tubular structures for conditions with

B2% and B5% (Figure 4b; Figure S5c, third row, Supporting Information). The cell number and percentage of area covered by cells remained constant (compared to mcFN^{wt}) using mcFN^{syn}, mcFN^{RGE}, and mcFN^{ARGD} in all conditions (B0%, B2%, and B5%). However, using mcFN^{RGE} and mcFN^{ARGD} the number of structures vanished only in B0% due to lack of cell alignment and fusion (Figure 4b, see insets; Figure S5d, Supporting Information). Note that for mcFN^{RGE} and mcFN^{ARGD} there is total lack of organization in absence of boron (B0%), so we were unable to quantify any parameters (Figure S5d, Supporting Information). In summary, simultaneous NaCB1 and VEGFR activation allowed the maintenance of comparable HUVEC organization levels between mcFN^{wt} and mcFN^{RGE}/mcFN^{ARGD} suggesting that enhanced VEGF/NaBC1 signaling is not dependent on $\alpha_5\beta_1$ and $\alpha_v\beta_3$ integrin binding.

2.7. Simultaneous NaBC1/VEGFR Stimulation Induces Receptor Colocalization

To test whether simultaneous stimulation of NaBC1 and VEGFR occurs through a synergistic cooperation mechanism produced by physical protein–protein interaction, we tested NaBC1/VEGFR colocalization using DUOLINK proximity ligation assay (PLA) system, which allows visualization of positive signals generated only if both receptors are within 40 nm distance. Figure 5a shows colocalization of NaBC1/VEGFR only after simultaneous stimulation with VEGF and boron. Little amounts of fluorescent dots were present also after VEGFR stimulation (B0%), but the dose-dependent increase of positive

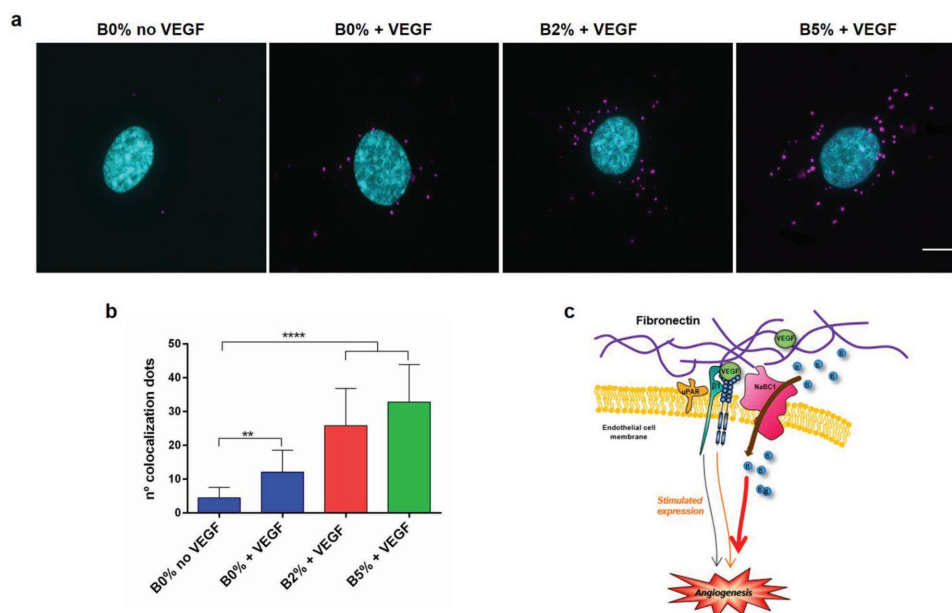


Figure 5. Colocalization of NaBC1 and VEGFR. a) Images of nuclei (cyan) and colocalization dots (magenta) of HUVEC cultured during 3 h onto functionalized substrates (FN-coated) with VEGF (25 ng mL⁻¹) and boron (B0%, B2%, and B5%) present in the culture medium. Scale bar represents 10 μ m. b) Image analysis quantification of colocalization dots of NaBC1/VEGFR. Colocalization levels increase as the stimulation of NaBC1 and VEGFR does. Statistics are shown as mean \pm standard deviation. $N = 30$ images per condition from three different biological replicas. Data were analyzed by an ordinary one-way ANOVA test and corrected for multiple comparisons using Dunnett analysis ($p = 0.05$). ** $p < 0.01$, **** $p < 0.0001$. c) Schematic representation of a NaBC1/VEGFR colocalization model, as a novel signaling mechanism, which involves cooperation between NaBC1 and VEGFR receptors after their respective activation to induce angiogenesis.

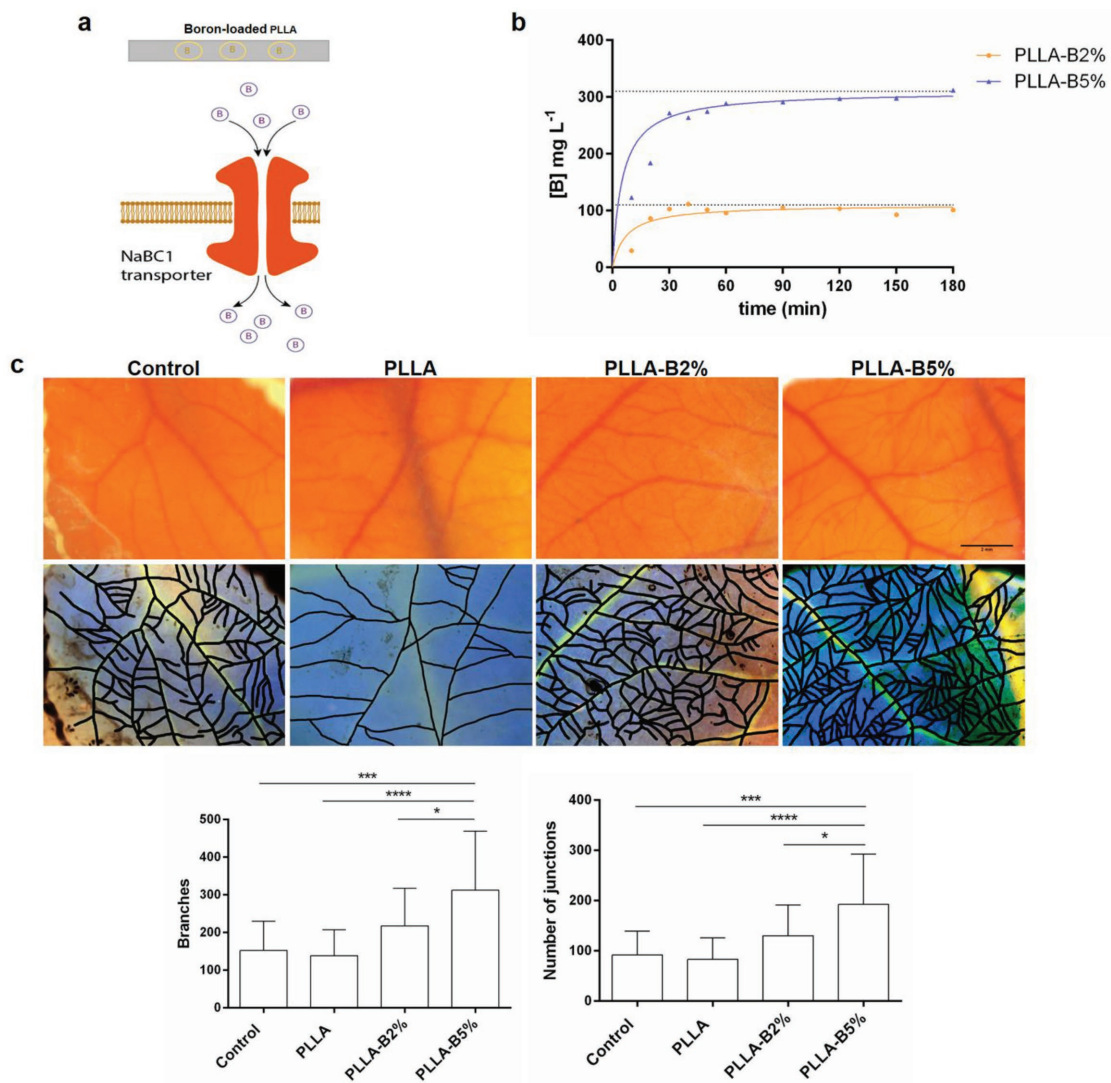


Figure 6. Boron release study and in vivo blood vessels formation on chick embryo chorioallantoic membrane (CAM). a) Scheme of boron-loaded PLLA release and boron transport inside the cell. b) Cumulative release of boron from PLLA–B2% and PLLA–B5%-loaded samples. Boron concentration was determined measuring A_{405} after azometin reaction. Final values were normalized with base absorbance values of bare PLLA. c) Representative stereomicroscope images of blood vessels formation after 96 h incubation with boron-loaded PLLA-functionalized substrates (PLLA–B2% and PLLA–B5%). Control samples correspond to physiological vasculogenesis on CAM without material and bare PLLA. Representative masks used for vessel quantification obtained after image treatment are shown in the lower row. Boron-loaded substrates significantly enhanced vasculogenesis in vivo. Image analysis quantification of total blood vessels formation expressed as branches, and the number of junctions indicating the levels of connection between the vessels. Statistics are shown as mean \pm standard deviation. $N = 20$ images per condition from six different biological replicas. Data were analyzed by an ordinary one-way ANOVA test and corrected for multiple comparisons using Tukey's analysis ($p = 0.05$). * $p < 0.05$, *** $p < 0.001$, **** $p < 0.0001$.

signals in the B2% and B5% conditions suggested that costimulation of both receptors is needed for effective colocalization (Figure 5b). Our results describe a novel protein–protein interaction between NaBC1 and VEGFR as a new mechanism for enhanced signaling in vascularization (Figure 5c).

2.8. Boron Induces In Vivo Vascularization

We have used PLLA, FDA-approved biodegradable material for a number of applications, as a support material for cells to grow in vitro and boron carrier to be released in vivo. We

used the chick embryo chorioallantoic membrane (CAM) assay to investigate the efficiency of NaBC1/VEGF signaling to promote vasculogenesis in vivo. CAM is an extra embryonic membrane that mediates nutrient and gas exchanges during the living period of embryo. It has been commonly used in vivo to study both angiogenesis and antiangiogenesis in response to cells, tumors or soluble factors.^[31] Figure 6a shows a schematic illustration of the concept of the system used for in vivo experiments. Figure 6b shows the cumulative release from boron-loaded PLLA solvent casted films, $\approx 100 \text{ mg L}^{-1}$ for PLLA–B2% and 300 mg L^{-1} for PLLA–B5%. We used these values to calculate the equivalent amount of boron added to the medium in

previous *in vitro* experiments (0.59×10^{-3} and 1.47×10^{-3} M as equivalent to PLLA–B2% and PLLA–B5%, respectively). We have used boron-loaded PLLA films that release boron within the first three hours after implantation (Figure 6b).

It is known that VEGF is already present in the chick embryo (chicken VEGF gene reference NM_001110355.1), and so we have used a system that releases boron, without any exogenous supplementation of VEGF.

PLLA films loaded with boron were deposited atop embryonic day 8 chicken CAM. After 96 h at 37.5 °C the total amount of blood vessels present was captured under a stereomicroscope. Figure 6c shows representative images of CAM vasculature and the correspondent masks created for image analysis. Boron delivery from PLLA (B2% and B5%)—in absence of exogenous VEGF—promoted neovascularization, with increased blood vessels formation and new interconnections (Figure 6c). Together, these data demonstrate that bioengineered systems that release boron promote vasculogenesis through a mechanism that suggests NaBC1/VEGF simultaneous signaling using VEGF already present in the host.

3. Discussion

Vascularization is a complex multistep event essential for cell survival, embryonic development, tissue repair, and fertility. It also plays a key role in tumor growth, invasion, and metastasis.^[1,3] In general, in all tissues after injury, the cell micro-environment turns hypoxic and loses the physiologic blood supply that acts as a source of oxygen, GFs, and cells needed for natural repair processes.

In regard to regenerative medicine, many tissue-engineered constructs had failed due to the inability to promote new vasculature.^[32] Thus, there is a real need to develop strategies that induced formation of a functional vascular supply.^[32–34] Current vascularization approaches involved GF delivery, cell delivery (or combined cell and GF delivery), as well as gene delivery^[33] using biomaterials as carriers. The use of GFs for therapeutic vascularization has been limited due to their use at supraphysiological doses that increases off-target side effects, including high cancer risk,^[5,34,35] as occurs with rhBMP2-infuse bone graft^[6] or PDGF (Regranex).^[7]

Other recent reported strategies to promote vascularization in bone tissue engineering use bioactive glasses that contain a variety of ions (i.e., Cu²⁺, Co²⁺, Ca²⁺, Si⁴⁺, B³⁺, Eu³⁺, and Mg²⁺). Released ions from bioactive glasses are the central elements participating in osteogenic response. However, vasculogenic response is only well documented for Cu²⁺ and Co²⁺, while for Ca²⁺, Si⁴⁺, B³⁺, Eu³⁺, and Mg²⁺, even if described that promote angiogenesis to some extent, the mechanism is not well defined.^[36] Indeed, bioactive glasses present low stability and uncontrolled release of multiple components that can present possible risks of soft tissue calcification. The specific mechanisms that accelerate neovascularization in the presence of the released ions from bioglass dissolutions have not yet been elucidated.^[36]

Here, we present a simple approach that promotes vascularization through a mechanism that involves simultaneous NaCB1 and VEGFR activation (Figure 1a), using boron to activate NaCB1 and promote the organization of HUVEC

(Figure 2a,b). Even if boron is not physiologically as abundant as other ions such as calcium or zinc, it is still essential in cell metabolism and has the potential to trigger cell differentiation *in vitro*.^[18] Ion-channel NaBC1^[19] is a unique and specific boron transporter that regulates the intracellular boron concentration. NaBC1 contains 14 transmembrane spans and multiple predicted intracellular phosphorylation sites for protein kinase A, protein kinase C, and calmodulin kinase II^[22] (Figure S1, Supporting Information). Here, we have predicted the NaBC1 3D-protein structural model and detected its expression in HUVEC (Figure 1b,c).

Blocking NaBC1 in the presence of boron resulted in a reduction of cell organization, and the effect was more pronounced with higher concentrations of boron (see B5% in Figure 2a,b and also Figure S3b in the Supporting Information demonstrating that NaBC1 activation is essential for enhanced HUVEC organization. Further, we showed that NaBC1 activation stimulated endothelial cell sprouting, which was prevented after blocking NaBC1 in the presence of boron (B2% and B5%, Figure 2c; Videos S1–S6, Supporting Information). This finding demonstrates that NaBC1/VEGFR simultaneous activation stimulates cell migration. Nevertheless, the precise role of NaBC1 transporter in modulating cell migration requires further investigation.

Akt is an essential protein kinase involved in various signaling cascades important in both normal cellular physiology and disease states. PI3K/Akt signaling pathway, specifically regarding endothelial cells, is activated (phosphorylated) by angiogenic GF and regulates downstream molecules involved in blood vessel growth and homeostasis controlling endothelial cell viability, NO-dependent vasodilation, and endothelial cell migration.^[37] Our *in cell western* results suggested that NaBC1 stimulation in combination with VEGF enhanced intracellular signaling via Akt phosphorylation (Figure 3b). After PI3k inhibition with LY-294002, HUVEC organization remained unaltered only in boron-containing systems (B2% and B5%) (Figure 3c; Figure S4c, Supporting Information). The fact that boron activation of NaBC1 rescued the effect of PI3k inhibition in HUVEC organization demonstrated that NaBC1 is involved in angiogenesis, enhancing Akt phosphorylation independently of PI3k, probably throughout activation of uPAR (Figure 4a), suggesting a novel interplay among NaBC1/VEGFR and uPAR.

To obtain further insights into this mechanism, we used mutant FNs that impaired $\alpha_5\beta_1$ and $\alpha_v\beta_3$ integrin binding.^[30] HUVEC organization was abrogated when substrates were coated with mcFN^{RGE} and mcFN^{ARGD} to prevent $\alpha_5\beta_1$ and $\alpha_v\beta_3$ binding (Figure 4b; Figure S5c,d, Supporting Information) but not in the presence of boron. It has been reported that VEGFR activate integrins through PI3k/Akt-dependent pathway,^[38] and integrin activation modulates regulation of PI3k/Akt.^[37,38] We show that either blocking PI3k or preventing integrin binding has no effect in NaCB1/VEGFR simultaneous signaling leading to enhanced vascularization in either case.

The fact that active NaBC1/VEGFR promoted HUVEC organization and sprouting in the absence of functional PI3k or $\alpha_5\beta_1/\alpha_v\beta_3$ binding, suggests that the mechanism is working through alternative routes to PI3k signaling for Akt phosphorylation. One explanation could be the activation of mammalian target of rapamycin (mTOR) pathway, another essential

metabolic road participating in vascularization, that after being stimulated by growth factors, increases Akt phosphorylation.^[37] Our data suggest that uPAR participates in VEGF-induced cell migration of endothelial cells via interaction with VEGFR, as previously reported.^[39] Then, blocking uPAR inhibits cell migration in a mechanism that is extracellular signal-regulated kinases (ERK) but not PI3K/Akt-dependent.^[13] Colocalization experiments demonstrate the physical interaction between NaBC1 and VEGFR (only positive signals appear if both proteins are located within 40 nm) (Figure 5a,b). For the first time, we demonstrated that NaBC1 acts as a novel molecular sensor, as occurs with other ion channels, and interact with the cytoplasmic environment and other membrane receptors such as integrins and growth factor receptors.^[15]

In summary, we demonstrated a novel function for NaBC1 ion channel stimulating intracellular signaling in coordination with VEGFR to induce enhanced vascularization (Figure 5c). These findings are supported by in vitro data providing mechanistic insights and, importantly, by in vivo data using CAM assays in the absence of exogenous VEGF (Figure 6c). Boron-active NaBC1 acts in synergy with VEGF membrane receptor stimulating intracellular signaling that promotes vasculogenesis and angiogenesis. These results open new possibilities for biomedical applications maximizing the effects of critical target receptors avoiding off-target effects produced by the use of supraphysiological doses of GFs.

4. Conclusions

This work shows, for the first time, that in order to fully potentiate the ability of biomaterials to control vascularization mechanisms, full attention needs to be given to the interplay between specific cell membrane receptors in order to mimic biological niche at molecular level. We hypothesize that simultaneous stimulation of NaBC1 and VEGF membrane receptors promote angiogenesis in the presence of ultralow doses of ligand (simulating physiological levels). We describe for the first time a novel vascularization mechanism that involves the crosstalk and colocalization between NaBC1 and VEGFR. We open new possibilities for the specific design of biomaterials at molecular level, avoiding the use of supraphysiological doses of growth factors causing adverse side effects and controlling critical target receptors instead.

5. Experimental Section

Material Substrates: PLLA (Cargill Dow) was dissolved at concentration of 2% (w/v) in chloroform. Borax 10 Mol ($\text{Na}_2\text{B}_4\text{O}_7 \cdot 10\text{H}_2\text{O}$) (Borax España S.A) was used to load materials and dissolved in the culture medium for all experiments performed. For abbreviation hereafter, it will be designated as boron. Different solutions of PLLA 2%, containing 2% and 5% of boron in relation to total mass of polymer ($m_T = m_{\text{PLLA}} + m_{\text{boron}}$), were performed in continuous stirring to prepare polymer sheets by the solvent casting method. After overnight chloroform evaporation, obtained films were dried in vacuo at 40 °C during 4 h and die-casted in 12 or 25 mm diameter substrates. These PLLA films (solvent casting) were used for in vivo experiments, and incorporated boron within the material.

PLLA 2% solution was used for substrate preparation of thin films by spin coating on cleaned glass cover slips for 30 s at 3000 rpm. Samples were dried at 60 °C in vacuo during 4 h.

Boron-Release Quantification: The in vitro release of boron was performed immersing different boron-loaded solvent-casted films (PLLA–boron-loaded 2% and 5%) in 1 mL of Dulbecco's phosphate-buffered saline (DPBS) (Sigma-Aldrich). PLLA was used as a control. Short terms accumulative release studies (maximum time 180 min) were performed removing a 40 μL aliquot from the medium every 10 min. A long-term release study was previously performed by describing that major release was produced during the first three hours of culture.^[18]

Reaction of boron present in the 40 μL aliquots with azometin (Sigma-Aldrich) in acid medium (KAc/HAc buffer pH 5.2) originated a colorimetric reaction measured at 405 nm in a Victor III (Perkin Elmer) device. Standards for calibration were prepared at concentrations of 0, 0.2, 0.3, 0.5, 1, 1.5, 2, 5.2, and 52 mg mL^{-1} of boron.

Mutant Fibronectin Production: Mutant FNs were obtained through different procedures in dependence of the different mutations. Due to the embryonic lethality of the deletion, homozygous $\text{FN}^{\text{ARGD}/\text{ARGD}}$ and $\text{FN}^{+/+}$ fibroblasts were generated from 3.5 days old (E3.5) blastocysts. The embryonic stem cells were induced to differentiate into fibroblasts after culturing in Dulbecco's modified Eagle's growth medium (DMEM, ThermoScientific) with 10% of fetal calf serum (FCS, ThermoScientific) and 1% dimethyl sulfoxide (DMSO, Sigma-Aldrich), immortalized by retroviral transduction of the SV-40 large T antigen, and cloned. The cell lines $\text{FN}^{\text{syn}/\text{syn}}$ and $\text{FN}^{\text{RGE}/\text{RGE}}$ were derived from E9.0 homozygous knock-in embryos^[30] and immortalized by the same procedure. All the cells were grown and maintained in DMEM medium with 10% fetal bovine serum (FBS, ThermoScientific) and 1% penicillin–streptomycin (GIBCO).

To purify mouse cellular fibronectin (mcFN), fibroblasts were grown until 100% confluence in DMEM with 10% FCS. Then, the medium was removed and washed three times with a serum replacement medium (SRM: 46.5% AIM-V, Life Technologies), 5% Roswell Park Memorial Institute medium (RPMI) (Life Technologies), and 1% nonessential amino acid (NEAA) solution (Sigma-Aldrich) and left overnight. The medium was again discarded and replaced by fresh SRM and collected every 2 days. $\text{cFN}^{\text{syn}/\text{syn}}$, cFN^{ARGD} , cFN^{RGE} , and cFN^{wt} were purified from the cell-conditioned SRM media as described previously with gelatin-Sepharose columns affinity chromatography.

Substrates' Functionalization: In all experiments, except the ones performed with mutant FN matrices, FN (Sigma-Aldrich) from hpFN was used as ECM protein. After sterilizing the samples with UV for 30 min, substrates were coated with FN solution for a concentration of 20 $\mu\text{g mL}^{-1}$ in DPBS during 1 h at room temperature (RT). The quantification of surface density of adsorbed FN,^[18] obtaining similar values for all boron-loaded or PLLA bare substrates disregarding any influence of boron on FN adsorption, was reported previously.

Wild-type and different mutant mcFNs were used for substrate coatings at 20 $\mu\text{g mL}^{-1}$ following the same procedure as hpFN.

HUVEC culture and Organization: HUVEC (Cellworks) were routinely maintained in human large vessel endothelial cell basal medium (HLVEC) supplemented with serum/antibiotics (Cellworks). Only cells between passages from 1 to 9 were used, and they were subcultured once a week before reaching confluence. In all experiments, cell-seeding density was 10.000 cells cm^{-2} . For HUVEC organization, cells were seeded over hpFN or mutant mcFN-coated substrates during 24 h at 37 °C and 5% CO_2 . After that, a fibrin 3D matrix composed of 20 mg mL^{-1} FG (Enzyme Research Laboratories), 50 U mL^{-1} of thrombin (Sigma-Aldrich), and 1.2 mg mL^{-1} of aprotinin (Sigma-Aldrich), all dissolved in HLVEC medium in absence of serum, was added. After 1 h at 37 °C to allow complete FG clotting, 3D matrix was covered with HLVEC complete media supplemented with 25 ng mL^{-1} of VEGF (R&D Systems) and boron (0.59×10^{-3} or 1.47×10^{-3} M, corresponding to the equivalent amount of boron in PLLA–boron 2% and 5% samples, respectively) where required. Cultures were maintained during 6 days.

In Cell Western: For evaluation of Akt phosphorylation, in cell western quantification was used. HUVEC (10,000 cells cm^{-2}) were seeded onto hpFN-coated substrates during 1.5 h at 37 °C and 5% CO_2 . After that, cells were fixed using fixative buffer (10 mL formaldehyde, 90 mL PBS, and 2 g sucrose) at 37 °C for 15 min and then permeabilized in cold methanol at 40 °C for 5 min. Cells were then blocked in 0.5% blocking buffer (nonfat dry milk powder in 0.1% phosphate buffered saline with Tween 20 (PBST) buffer) at RT for 2 h followed by three washes of 10 min with 0.1% PBST. Cells were then incubated with primary antibodies at 1:100 dilution in blocking buffer at 4 °C over night separately: Akt (ThermoFisher) and pAkt (ThermoFisher). After three washes of 10 min with 0.1% PBST buffer, cells were incubated with 1:800 diluted infrared-labeled secondary antibody IRDye 800CW (LI-COR) and 1:500 diluted CellTag 700 Stain (LI-COR) at RT for 1 h, followed by five washes of 10 min with 0.1% PBST. Samples were then dried overnight at RT. Infrared signal was detected using an Odyssey infrared imaging system.

Intracellular Signaling Blocking: For PI3K specific inhibition, LY-294002 (Sigma-Aldrich) was used at a concentration of 40×10^{-6} M. 24 h after cell seeding and addition of Fibrin 3D matrix, HLVEC medium was supplemented once with LY-294002. After 2 days medium was changed normally without further LY-294002 addition until the end of culture.

NaBC1 Blocking: For boron transporter blocking, a specific antibody was used against a synthetic peptide corresponding to internal amino acids 109–123 of human sodium bicarbonate transporter-like protein 11 (NP_114423.1, SLC4A11), or NaBC1 (abcam).

Cells were seeded, and HLVEC media were supplemented with NaBC1 antibody at a final concentration of $1 \mu\text{g mL}^{-1}$. All medium changes were supplemented with antibody when needed until the end of culture.

NaBC1 3D Molecular Modeling: The search for templates in PDB database revealed the human erythrocyte band 3 protein SLC4A1 (Protein bank codes 4YZF and 4KY9 for the cytosolic and the anion exchanger domains, respectively) as the best match to model the boron transporter named *Homo sapiens* bicarbonate transporter-related protein BTR1 (AF336127.1), with a sequence similarity of around 30%. 3D-protein structural models were obtained with the SWISS-MODEL server in Automated Model. Structural figures were drawn using PyMol (<https://www.pymol.org>). In the absence of a full structural model of SLC4A1, the relative positions of the cytosolic and the anion exchanger domains were drawn arbitrarily.

Sequence and structural alignment figure of diverse anion transporters (AE4, NBC1, NDCBE1, and BTR1) were obtained with ClustalX and <http://esript.ibcp.fr>.

Gene Expression: Total RNA was extracted from HUVEC cultured for 6 days under different experimental conditions using RNeasy micro kit (Qiagen). RNA quantity and integrity was measured with a NanoDrop 1000 (ThermoScientific). Then 500 ng of RNA was reverse transcribed using the Superscript III reverse transcriptase (Invitrogen) and oligo dT primer (Invitrogen). Real-time qPCR was performed using Sybr select master mix and 7500 Real Time PCR system from Applied Biosystems. The reactions were run at least in triplicate for both technical and biological replicas. The primers used for amplification were designed based on sequences found in the GenBank database and included: integrin α_5 (NM_002205.4, forward: 5'-GGA CTG TGG AGA AGA CAA CAT C-3', reverse: 5'-GTG AGG TTC AGG GCA TTC TT-3'), integrin β_1 (NM_002211.3, forward: 5'-ATC CCA TTG ACC TCT ACT ACC T-3', reverse: 5'-GTC CGA AGT AAT CCT CCT CAT TT-3'), integrin α_x (NM_002210.4, forward: 5'-TAG CAA CTC CCA CTG CAC AAG CTA-3', reverse: 5'-AAC CAT TCC CAA AGT CCT TGC TGC-3'), integrin β_3 (NM_000212.2, forward: 5'-CAT CCA TAG CAC CTC CAC ATA C-3', reverse: 5'-CCA GCC AAC TCA TGG GAA TAA-3'), uPA (NM_002658, forward: 5'-GTG GAT GTG CCC TGA AGG A-3', reverse: 5'-TGC GGA TCC AGG GTA AGA AG-3'), uPAR (NM_002659, forward: 5'-CCC AAT CCT GGA GCT TGA AA-3', reverse: 5'-TTG GTT TTT CGG TTC GTG AGT-3'), β -actin (NM_001101.3, forward: 5'-CGC CGC CAG CTC ACC ATG-3', reverse: 5'-CAC GAT GGA GGG GAA GAC GG-3').

The fractional cycle number at which fluorescence passed the threshold (C_t values) was used for quantification using the comparative

C_t method. Sample values were normalized to the threshold value of housekeeping gene β -actin: $\Delta C_t = C_t$ (experiments) - C_t (β - actin). The C_t value of the control (B0% substrate) was used as a reference. $\Delta\Delta C_t = \Delta C_t$ (experiment) - ΔC_t (control). mRNA expression was calculated by the following equation: fold change = $2^{-\Delta\Delta C_t}$.

NaBC1 PCR detection was performed using AmpliTaq Gold 360 DNA polymerase (Invitrogen). The primers used for amplification were designed based on sequences found in the GenBank database (AF336127.1, forward: 5'-CAT GAT CGC CAT GAT CCC CAT CCG-3', reverse: 5'-CAG ATG CCC CAG GCC TGA GTC AGC-3').

Colocalization Experiments: Colocalization of NaBC1/VEGFR experiments was performed using DUOLINK PLA system (Sigma-Aldrich) and following manufacturer instructions. Specific primary antibodies used were anti NaBC1 (dilution 1:200, abcam) and anti VEGFR (dilution 1:400, abcam). For image quantification of colocalization fluorescent dots, at least 20 individual cells were imaged for each condition under an epifluorescence microscope (Nikon Eclipse 80i).

CAM Assay: Chick CAM assay was tested for vascularization potential of different boron-loaded materials. Boron-loaded PLLA (solvent casted) was previously characterized and it was confirmed that boron does not change surface wettability, mechanical properties, or the amount of FN adsorbed compared to PLLA.^[18]

PLLA, PLLA-B2%, and PLLA-B5% solvent-casted films were grafted atop chorioallantoic membrane from embryonic day 8 chicken. Chorioallantoic membrane without material was used as control condition. Total blood vessels were imaged with a stereomicroscope after 96 h of incubation at 37.5 °C.

Image Analysis: The 8-bit monochrome fluorescence images corresponding to HUVEC and nuclei 4',6-diamino-2-phenylindol (DAPI) were segmented using an interactive semiautomatic machine-learning algorithm with Ilastik 1.2.2. Background and cells were segmented and converted to a binary mask in Fiji-ImageJ. The contours were softened applying a 3 pixel wide Gaussian blur filter followed by a binarization filter. Then, the masks were skeletonized and the skeleton parameters were analyzed using the Analyze skeleton plugin in Fiji-ImageJ.

For the CAM assay, the stereomicroscope RGB color images were enhanced using histogram normalization on the three channels using Fiji-ImageJ and the vessels were marked manually to allow segmentation. The images with the marked vessels were thresholded to isolate the markings from the background and obtain a binary image. The binary image was skeletonized and analyzed using the Analyze skeleton plugin of Fiji-ImageJ.

The following parameters of the skeletonized binary masks were analyzed: junctions, slab pixels, total number of triple points, number of cells, total cell area, and percentage of area covered by cells. The total number of structures, defined as isolated groups of branches in the skeletonized image, was also determined. A minimum of ten microscope fields per experimental condition were analyzed.

Statistical Analysis: For statistical analysis, the data were analyzed for normality using the D'Agostino and Pearson omnibus normality test with an α of 0.05. When the normality test was passed, an ordinary one-way analysis of variance (ANOVA) test with a Tukey's, Sidak's, or Dunnett's posthoc analysis ($p = 0.05$) was used to compare the means of the columns against the control column. When the normality test was not passed, a nonparametric test with a posthoc Dunn analysis ($p = 0.05$) was used to compare the means of each column against the control column. Data were represented as mean \pm standard deviation (SD). Sample size for each statistical analysis was indicated in the corresponding figure legends. GraphPad Prism 6 XML software was used for statistical analysis.

Supporting Information

Supporting Information is available from the Wiley Online Library or from the author.

Data Availability

The datasets generated during and/or analyzed during the current study are available in the University of Glasgow Repository, <http://dx.doi.org/10.5525/gla.researchdata.685>.

Acknowledgements

P.R. acknowledges support from the Ministerio de Economía, Industria y Competitividad, Gobierno de España (MINECO) (MAT2015-69315-C3-1-R), and European Regional Development Fund (FEDER). CIBER-BBN is an initiative funded by the VI National R&D&I Plan 2008–2011, Iniciativa Ingenio 2010, Consolider Program, CIBER Actions and financed by the Instituto de Salud Carlos III with assistance from the European Regional Development Fund. M.S.S. acknowledges support from the European Research Council (ERC—HeallnSynergy 306990) and the UK Engineering and Physical Sciences Research Council (EPSRC—EP/P001114/1). The authors are very grateful to Productos Florida farm for kindly providing chick embryos for CAM assay.

Conflict of Interest

The authors declare no conflict of interest.

Keywords

boron ion, fibronectin, integrins, NaBC1, vascularization, VEGF

Received: July 12, 2018

Revised: October 6, 2018

Published online:

- [1] G. D. Yancopoulos, S. Davis, N. W. Gale, J. S. Rudge, S. J. Wiegand, J. Holash, *Nature* **2000**, 407, 242.
- [2] P. Carmeliet, *Nature* **2005**, 438, 932.
- [3] V. Moulisová, C. Gonzalez-García, M. Cantini, A. Rodrigo-Navarro, J. Weaver, M. Costell, R. Sabater i Serra, M. J. Dalby, A. J. García, M. Salmerón-Sánchez, *Biomaterials* **2017**, 126, 61.
- [4] P. S. Briquez, L. E. Clegg, M. M. Martino, F. M. Gabhann, J. A. Hubbell, *Nat. Rev. Mater.* **2016**, 1, 15006.
- [5] J. R. Hanft, R. A. Pollak, A. Barbul, C. van Gils, P. S. Kwon, S. M. Gray, C. J. Lynch, C. P. Semba, T. J. Breen, *J. Wound Care* **2008**, 17, 30.
- [6] E. J. Woo, *Spine J.* **2012**, 12, 894.
- [7] United States Food and Drug Administration, Product Description Regranex, <https://www.fda.gov/downloads/Drugs/Drug-Safety/PostmarketDrugSafetyInformationforPatientsandProviders/UCM142821.pdf>, (accessed: May 2008).
- [8] P. Carmeliet, R. K. Jain, *Nature* **2011**, 473, 298.
- [9] R. O. Hynes, *Cell* **2002**, 110, 673.
- [10] G. H. Mahabeleshwar, W. Feng, K. Reddy, E. F. Plow, T. V. Byzova, *Circ. Res.* **2007**, 101, 570.
- [11] A. K. Olsson, A. Dimberg, J. Kreuger, L. Claesson-Welsh, *Nat. Rev. Mol. Cell Biol.* **2006**, 7, 359.
- [12] R. A. Alexander, G. W. Prager, J. Mihaly-Bison, P. Uhrin, S. Sunzenauer, B. R. Binder, G. J. Schütz, M. Freissmuth, J. M. Breuss, *Cardiovasc. Res.* **2012**, 94, 125.
- [13] S. Herkenne, C. Paques, O. Nivelles, M. Lion, K. Bajou, T. Pollenus, M. Fontaine, P. Carmeliet, J. A. Martial, N. Nguyen, I. Struman, *Sci. Signaling* **2015**, 8, 1.
- [14] I. Lauritzen, J. Chemin, E. Honoré, J. Martine, N. Guy, M. Lazdunski, A. J. Patel, *EMBO Rep.* **2005**, 6, 642.
- [15] A. N. Gasparski, K. A. Beningo, *Arch. Biochem. Biophys.* **2015**, 586, 20.
- [16] L. Munaron, T. Genova, D. Avanzato, S. Antoniotti, A. Fiorio Pla, *Recent Pat. Anti-Cancer Drug Discovery* **2013**, 8, 27.
- [17] X. Yao, C. J. Garland, *Circ. Res.* **2005**, 97, 853.
- [18] P. Rico, A. Rodrigo-Navarro, M. Salmerón-Sánchez, *Tissue Eng., Part A* **2015**, 21, 2662.
- [19] M. Park, Q. Li, N. Shcheynikov, W. Zeng, S. Muallem, *Mol. Cell* **2004**, 16, 331.
- [20] E. N. Vithana, P. Morgan, P. Sundaresan, N. D. Ebenezer, D. T. Tan, M. D. Mohamed, S. Anand, K. O. Khine, D. Venkataraman, V. H. Yong, M. Salto-Tellez, A. Venkataraman, K. Guo, B. Hemadevi, M. Srinivasan, V. Prajna, M. Khine, J. R. Casey, C. F. Inglehearn, T. Aug, *Nat. Genet.* **2006**, 38, 755.
- [21] I. A. Lopez, M. I. Rosenblatt, C. Kim, G. C. Galbraith, S. M. Jones, L. Kao, D. Newman, W. Liu, S. Yeh, A. Pushkin, N. Abuladze, I. Kurtz, *J. Biol. Chem.* **2009**, 284, 26882.
- [22] M. D. Parker, E. P. Ourmozdi, M. J. Tanner, *Biochem. Biophys. Res. Commun.* **2001**, 282, 1103.
- [23] R. Zangi, M. Filella, *Chem.-Biol. Interact.* **2012**, 197, 47.
- [24] H. Tanjore, E. M. Zeisberg, B. Gerami-Naini, R. Kalluri, *Dev. Dyn.* **2008**, 237, 75.
- [25] H. P. Gerber, V. Dixit, N. Ferrara, *J. Biol. Chem.* **1998**, 273, 13313.
- [26] C. Tan, S. Cruet-Hennequart, A. Troussard, L. Fazli, P. Costello, K. Sutton, J. Wheeler, M. Gleave, J. Sanghera, S. Dedhar, *Cancer Cell* **2004**, 5, 79.
- [27] E. L. George, H. S. Baldwin, R. O. Hynes, *Blood* **1997**, 90, 3073.
- [28] R. Fässler, M. Meyer, *Genes Dev.* **1995**, 9, 1896.
- [29] R. Soldi, S. Mitola, M. Strasly, P. Defilippi, G. Tarone, F. Bussolino, *EMBO J.* **1999**, 18, 882.
- [30] S. Takahashi, M. Leiss, M. Moser, T. Ohashi, T. Kitao, D. Heckmann, A. Pfeifer, H. Kessler, J. Takagi, H. P. Erickson, R. Fässler, *J. Cell Biol.* **2007**, 178, 167.
- [31] D. Ribatti, *Int. Rev. Cell Mol. Biol.* **2008**, 270, 181.
- [32] E. C. Novosel, C. Kleinhans, P. J. Kluger, *Adv. Drug Delivery Rev.* **2011**, 63, 300.
- [33] J. García, A. J. García, *Drug Delivery Transl. Res.* **2016**, 6, 77.
- [34] P. S. Briquez, J. A. Hubbell, M. M. Martino, *Adv. Wound Care* **2015**, 4, 479.
- [35] T. Simon-Yarza, F. R. Formiga, E. Tamayo, B. Pelacho, F. Prosper, M. J. Blanco-Prieto, *Theranostics* **2012**, 2, 541.
- [36] S. Kargoza, F. Bains, S. Hamzehlou, R. G. Hill, M. Mozafari, *Trends Biotechnol.* **2018**, 36, 430.
- [37] M. Laplante, D. M. Sabatini, *J. Cell Sci.* **2009**, 122, 3589.
- [38] T. V. Byzova, C. K. Goldman, N. Pampori, K. A. Thomas, A. Bett, S. J. Shattil, E. F. Plow, *Mol. Cell* **2000**, 6, 851.
- [39] R. A. Alexander, G. W. Prager, J. Mihaly-Bison, P. Uhrin, S. Sunzenauer, B. R. Binder, G. J. Schutz, M. Freissmuth, J. M. Breuss, *Cardiovasc. Res.* **2012**, 94, 125.